Water follows carbon: CO_2 incites deep silicate melting and dehydration beneath mid-ocean ridges

Rajdeep Dasgupta*
Marc M. Hirschmann
Neil D. Smith
Department of Geology and Geophysics, University of Minnesota, 310 Pillsbury Drive SE, Minneapolis, Minnesota 55455, USA

ABSTRACT

Hydrous defects in nominally anhydrous minerals influence the physical properties and reduce the melting point of mantle rocks. Consequently, it is believed that extraction of H_2O beneath mid-ocean ridges by dehydration melting enhances the creep strength of the upper mantle and produces a chemical lithosphere. However, recent studies show that trace water induces melting at shallower depths beneath ridges than previously believed. Here we explore the hypothesis that incipient melting, dehydration, and strengthening of the subridge mantle is promoted by trace quantities of carbon. Experiments at 3 GPa on carbonated peridotite with 1 and 2.5 wt% CO_2 produce partial melts that change from carbonatites with <10 wt% SiO_2 to carbonated silicate melts with >25 wt% SiO_2 between 1325 and 1350 °C. Enhanced melting of carbonated peridotite relative to volatile free peridotite is parameterized as a simple function of the concentration of CO_2 in the melt. Application of this model to mantle with 100 ppm bulk CO_2 suggests that the subridge mantle undergoes silicate melting ~130–140 °C below the CO_2-free solidus, corresponding to a depth of ~110 km beneath ridges, and that 0.2 wt% partial melting will be attained at a depth of ~75 km. The combined effects of H_2O and CO_2 further enhance deep silicate melting, as H_2O partitions from nominally anhydrous silicates to carbonated silicate melts. Thus, the deepest silicate melting beneath ridges will be induced by the combination of H_2O and CO_2, rather than simply by dehydration melting of nominally anhydrous peridotite, and this combination is likely responsible for dehydration strengthening of the oceanic lithosphere and for geochemical signatures of deep melting in mid-oceanic ridge basalt.

Keywords: mid-oceanic ridge, partial melting, lithosphere, mantle volatiles, CO_2, dehydration.

INTRODUCTION

The onset and the extent of partial melting beneath ridges are of great importance to geochemical and geophysical processes at divergent plate margins. The pioneering work of Hirth and Kohlstedt (1996) demonstrated the importance of dehydration to deep partial melting beneath ridges. Dehydration enhances the strength of residual mantle minerals, resulting in formation of a strong chemical lithosphere (Hirth and Kohlstedt, 1996; Evans et al., 2005) and influencing the dynamics of mantle flow beneath ridges (Braun et al., 2000; Choblet and Parmentier, 2001). The deep onset of small-degree melting owing to H_2O influences the composition of mid-ocean ridge basalt (MORB), enhancing the contribution of deep small-degree melts without greatly increasing the thickness of oceanic crust produced (Asimow and Langmuir, 2003). Deep melting influences the seismological and electrical conductivity structure of the subridge mantle, and therefore may be required to explain geophysical features observed during the Mantle Electromagnetic and Tomography (MELT) experiment (Forsyth et al., 1998; Evans et al., 1999, 2005).

A key parameter is the depth of melting-induced dehydration, which is related to the depth at which volatile-induced melting yields a melt fraction sufficient to extract most H_2O from the residue. Quantitative models of hydrous melting (Hirth and Kohlstedt, 1996; Asimow and Langmuir, 2003; Katz et al., 2003; Aubaud et al., 2004) differ in their predictions, in part because they are based on indirect experimental constraints. Hirth and Kohlstedt (1996) predicted that for a subridge adiabat that crosses the dry solidus of peridotite at ~60 km, 150 ppm H_2O should induce melting beginning at 115 km depth; however, as illustrated in Figure 1, they predict considerable dehydration melting at temperatures well below those predicted by more recent models. The differences may arise in part because Hirth and Kohlstedt (1996) underestimated the storage capacity of H_2O in olivine by a factor of ~3 (Bell et al., 2003). Thus, the influence of small amounts of H_2O on deep melting, geophysical properties beneath ridges, and the geochemistry of MORB may be less potent than inferred by Hirth and Kohlstedt (1996).

The deepest melting beneath ridges is likely a tiny fraction (<0.1%) of carbonatite released as deep as 300 km, which may remove only a small amount (<10%) of the H_2O from the residual peridotite (Dasgupta and Hirschmann, 2006). At shallower depths, CO_2 may stabilize carbonated silicate partial melts (Wendlandt and Mysen, 1980; Hirose, 1997). Compared to carbonatites, such melts have much lower CO_2 concentrations and so can yield much larger melt fractions, which in turn may remove greater proportions of H_2O. Here we present new experimental data on generation of silicate melts from carbonated peridotite and develop a model for generation of such melts from peridotite with trace CO_2 concentrations. We show that extraction of CO_2-bearing silicate melts occurs at depths similar to or greater than the initiation of dehydration melting. This may be a principal influence on deep melting and extraction of water beneath ridges.

METHODS

Carbonated peridotites containing 2.5 (PERC) and 1 wt% CO_2 (PERC3) were constructed from mixtures of natural silicate and carbonate minerals and reagent carbonates. To minimize contamination from H_2O, carbonate compounds were fired in a 1 atm furnace at 250–300 °C

*Current address: Lamont-Doherty Earth Observatory, Columbia University, 61 Route 9W, Palisades, New York 10964, USA; E-mail: rajdeep@ldeo.columbia.edu.

© 2007 Geological Society of America. For permission to copy, contact Copyright Permissions, GSA, or editing@geosociety.org.

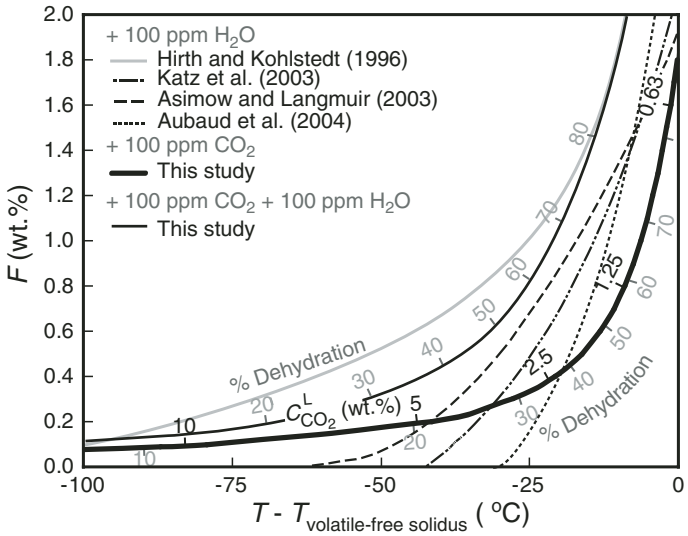


Figure 1. Models of dehydration melting of peridotite (Hirth and Kohlstedt, 1996; Asimow and Langmuir, 2003; Katz et al., 2003; Aubaud et al., 2004) calculated at 3 GPa for 100 ppm H_2O showing melt fraction (*F*) in weight percent vs. reduced temperature (*T*), defined as $T - T_{\text{volatile-free solidus}}$ (°C). Also shown are calculated melt fractions for peridotite + 100 ppm CO_2 and for peridotite with 100 ppm H_2O and 100 ppm CO_2, as described in text. Numbers in black and gray along curve for peridotite + 100 ppm CO_2 indicate, respectively, concentration of CO_2 (wt%) in melt and percent dehydration of residual peridotite matrix assuming fractional melting and $D^{\text{peridotite/melt}}_{H_2O} = 0.009$. Percent dehydration of residual peridotite is also shown for peridotite + H_2O + CO_2 curve.

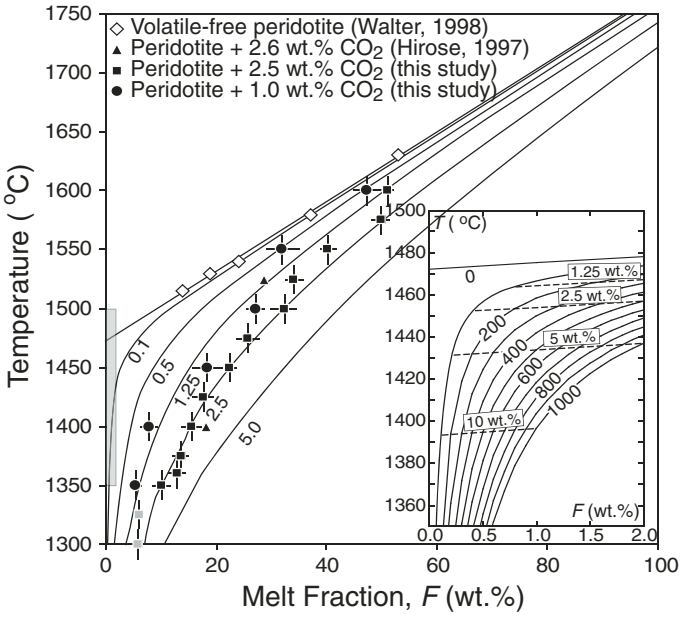


Figure 2. Temperature (*T*) vs. melt fraction (*F*) determined at 3 GPa for partial melting of peridotite ± CO_2. Experimental melt fractions are for PERC (filled squares: gray—carbonatite, black—carbonated silicate melt) and PERC3 (filled circles) carbonated peridotite (see text) and for KLB-1 + 5 wt% magnesite (filled triangles; data from Hirose, 1997). Data for CO_2-free peridotite (open diamonds) are from Walter (1998). Contours of *F* vs. *T* for peridotite with bulk CO_2, $C^0_{CO_2}$, ranging from 0.1 to 5 wt%, are derived from parameterization described in text. Inset shows expanded view of low melt fraction region near volatile-free peridotite solidus (gray shaded box) with contours of *F* vs. *T* for $C^0_{CO_2}$ ranging between 100 and 1000 ppm and illustrates that small amounts of CO_2 induce small-degree silicate partial melts well below volatile-free solidus. Dashed curves are isopleths of CO_2 in melt, $C^L_{CO_2}$. CO_2-free *T-F* trend may be slightly curved between 0% and 5% melting (Hirschmann et al., 1999), which would also displace *T-F* trends of CO_2-bearing isopleths downward, but would not affect appreciably estimates of difference in temperature between CO_2-induced melting and CO_2-free melting at any given fraction.

for 4–12 h before mixing with silicates. For further details of preparation and bulk compositions, see Dasgupta and Hirschmann (2006). To ensure nominally anhydrous conditions, homogeneous mixtures of silicates and carbonates were loaded in platinum-graphite capsules and kept in a drying oven at 120 °C for 2–4 h prior to welding the outer platinum capsule. Partial melting experiments were performed at 3 GPa (Table 1) in an end-loaded piston-cylinder device using the procedures described in Dasgupta et al. (2005). Mineral and melt compositions were analyzed with an electron microprobe and are reported elsewhere.

RESULTS

The subsolidus assemblage for PERC includes olivine, orthopyroxene, clinopyroxene, garnet, and dolomite (Dasgupta and Hirschmann, 2006). Above the solidus (≥1075 °C), crystalline carbonate disappears and carbonatitic melt is present up to 1325 °C. For both bulk compositions, a sharp transition from carbonatite (<10 wt% SiO_2, ≥40 wt% CO_2) to carbonated silicate melts (>25 wt% SiO_2, <25 wt% CO_2) is observed between 1325 and 1350 °C (Table 1). Between the solidi and ~1330 °C, carbonatitic melt fractions remain nearly constant, but once silicate melting commences, melt fractions increase sharply, corresponding to a rapid transition from carbonate melts to CO_2-rich silicate melts. Further increases in temperature cause melt fractions to increase (Fig. 2), with corresponding dilution in CO_2 and enrichment in SiO_2 (Table 1).

DISCUSSION

In the presence of CO_2, appreciable melting of mantle silicates begins at temperatures significantly below the volatile-free solidus (Fig. 2). However, the subridge mantle likely contains as little as 100 ppm CO_2 (Marty and Tolstikhin, 1998), and the extent of CO_2-induced melting is proportional to the available CO_2, $C^0_{CO_2}$. Determining the effect of CO_2 on melting of natural peridotites with 100s of ppm CO_2 requires extrapolation from experimental results with relatively CO_2-rich bulk compositions. To estimate the extent of silicate melting, *F*, induced by trace amounts of CO_2, we parameterize the temperature difference, ΔT, at a given melt fraction between the *T-F* trends for volatile-free peridotite (Walter, 1998) and for carbonated peridotite (this study; also see Hirose, 1997) as a function of CO_2 content of the experimental melts, $C^L_{CO_2}$ (Fig. 3). The $C^L_{CO_2}$ versus ΔT trend is nearly linear up to ~25 wt% CO_2, consistent with simple freezing point depression (Denbigh, 1981). It can be fitted with an empirical function

$$\Delta T\ (°C) = 27.04 \times C^L_{CO_2} + 1490.75 \times \ln\left[(100 - 1.18 \times C^L_{CO_2})/100\right] \quad (1)$$

where $C^L_{CO_2}$ is in weight percent. Assuming that CO_2 is essentially incompatible in silicate minerals ($D^{\text{peridotite/melt}}_{CO_2}$ <~10^{-4} for silicate melts and ~10^{-5} for carbonate melts; Hauri et al., 2006; Shcheka et al., 2006), equation 1 allows calculation of *T-F* trends for peridotite with variable bulk concentrations of CO_2 (Fig. 2).

Compared to recent models of dehydration-induced melting for 100 ppm H_2O (Asimow and Langmuir, 2003; Katz et al., 2003; Aubaud et al., 2004), 100 ppm CO_2 induces small amounts of silicate melting at lower temperatures (Fig. 1). At 3 GPa, silicate melting (<25 wt% CO_2, >25 wt% SiO_2; Table 1) of carbonated peridotite begins ~140 °C below the volatile-free peridotite solidus (Fig. 2), though the melt fraction is tiny (~0.04% for 100 ppm CO_2 in bulk peridotite). The proportion of carbonated silicate melt increases to 0.1, 0.2, and 0.5 wt% at 80, 40, and 15 °C, respectively, below the volatile-free solidus (Fig. 1).

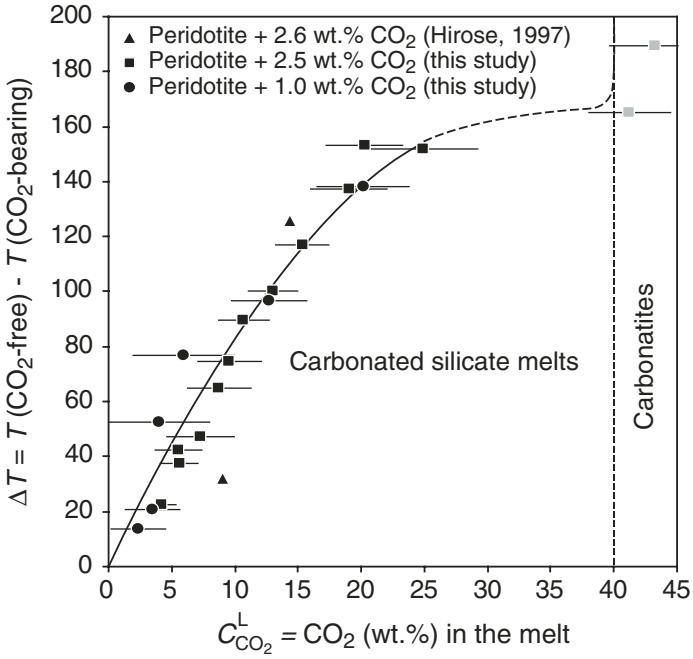


Figure 3. Concentration of CO_2 in partial melts of carbonated peridotite, $C^{L}_{CO_2}$, vs. ΔT, where ΔT is defined as difference between temperature at which volatile-free peridotite achieves melt fraction (F) observed in experiment (at 3 GPa) and temperature of experiment. Former is derived from T-F trend defined by experiments of Walter (1998), as depicted in Figure 2 and defined by line T (°C) = 2.95 × F (wt%) + 1472.3. Data from peridotite + CO_2 are from this study, with $C^{L}_{CO_2}$ estimated from microprobe totals (Table 1) and from Hirose (1997), with $C^{L}_{CO_2}$ estimated from melt fractions (calculated from mass balance) and total CO_2, $C^{0}_{CO_2}$, assuming that CO_2 is completely incompatible in silicates. Symbols are as in Figure 2 and error bars in CO_2 concentrations are based on replicate probe analyses. Solid line is from equation 1 in text; dashed curve from ≥25 wt% to ~40 wt% CO_2 is hand-drawn and indicates sharp transition from carbonatite to carbonated silicate liquids.

TABLE 1. SUMMARY OF 3 GPa PARTIAL MELTING EXPERIMENTS

Run No.	Temp. (°C)	Time (hr)	Phases (Ol+Opx+)	Melt fraction (wt%)	CO_2 (melt) (wt%)	SiO_2 (melt) (wt%)
PERC (peridotite+2.5 wt.% CO_2)						
A469	1075	95	Cpx, Gt, Dol	—	—	—
A470	1105	72	Cpx, Gt, cbL	n.d.	n.d.	n.d.
A471	1300	24	Cpx, Gt, cbL	6.0 ± 0.3	43.8 ± 2.1	5.3 ± 1.5
A472	1325	24	Cpx, Gt, cbL	6.2 ± 0.3	41.1 ± 2.1	7.0 ± 1.5
A501	1340	48	Cpx, Gt, sL	n.d.	n.d.	n.d.
A482	1350	24	Cpx, Gt, sL	10.1 ± 1.6	24.9 ± 4.3	28.4 ± 6.9
A500	1360	48	Gt, sL	13.1 ± 1.4	20.3 ± 3.0	32.3 ± 5.3
A483	1375	24	Gt, sL	13.7 ± 1.3	19.0 ± 3.0	32.0 ± 4.9
A486	1400	24	Gt, sL	15.5 ± 1.8	15.4 ± 2.1	34.5 ± 4.5
A488	1425	24	Gt, sL	17.7 ± 1.8	13.0 ± 2.0	35.8 ± 4.5
A490	1450	24	sL	22.5 ± 1.1	10.7 ± 2.0	37.4 ± 3.1
A491	1475	24	sL	25.8 ± 2.2	9.6 ± 2.5	40.2 ± 3.0
A492	1500	24	sL	32.3 ± 2.3	8.8 ± 2.5	41.3 ± 3.5
A494	1525	24	sL	34.1 ± 1.5	7.3 ± 2.7	42.6 ± 1.7
A493	1550	6	sL	40.3 ± 1.3	5.6 ± 1.5	45.4 ± 1.5
A495	1575	6	sL (no Opx)	49.8 ± 1.5	5.5 ± 1.9	45.6 ± 1.2
A496	1600	4	sL (no Opx)	51.0 ± 1.1	4.2 ± 1.2	45.6 ± 0.8
PERC3 (peridotite+1.0 wt.% CO_2)						
A509	1350	24	Cpx, Gt, sL	5.5 ± 0.9	20.2 ± 3.7	42.8 ± 3.8
A510	1400	25	Cpx, Gt, sL	7.8 ± 1.4	12.7 ± 3.0	43.8 ± 3.5
A520	1425	25	sL	n.d.	n.d.	n.d.
A512	1450	25	sL	20.7 ± 2.6	6.0 ± 4.0	44.0 ± 4.4
A514	1500	23	sL	27.1 ± 1.6	4.0 ± 4.0	45.4 ± 4.0
A515	1550	7	sL	32.0 ± 2.9	3.5 ± 2.2	47.5 ± 3.3
A516	1600	4	sL	47.2 ± 2.4	2.4 ± 2.2	48.1 ± 3.0

Note: Ol—olivine, Opx—orthopyroxene, Cpx—clinopyroxene, Gt—garnet, Dol—dolomite solid solution, cbL—carbonatite melt, sL—CO_2-bearing silicate melt, n.d.—not determined. Melt fractions estimated by mass balance calculations from compositions of the observed phases and of the starting mix. Errors are 1σ and for melt fractions are estimated from variations of phase compositions in replicate analyses. CO_2 concentrations in melt are estimated from microprobe totals.

If CO_2 and H_2O could be considered separately, then comparison of our results to the dehydration melting models of Asimow and Langmuir (2003), Katz et al. (2003), and Aubaud et al. (2004) would suggest that for a subridge source with ~100 ppm H_2O (Michael, 1988) and ~100 ppm CO_2, CO_2 would initiate the first ~0.2%–0.3% of silicate melting and H_2O would be chiefly responsible for higher degrees of melting (Fig. 1). This suggests that the deepest silicate melting beneath ridges is likely induced by CO_2, rather than H_2O. The volatiles do not act separately. H_2O segregates into the carbonated silicate melts owing to incompatible behavior during melting, and the resulting H_2O dissolved in the melt thereby enhances the freezing point depression of CO_2 acting alone.

Given an estimate of the partitioning of H_2O between nominally anhydrous peridotite and carbonated silicate melts, $D_{H_2O}^{peridotite/melt}$, the extent of H_2O extraction due to carbonated silicate melting and the associated extra freezing point depression can be estimated. Although $D_{H_2O}^{peridotite/melt}$ is not known for carbonated silicate melts, dissolved CO_2 does not have a strong effect on the energetics of H_2O solution in silicate melts (Papale, 1999), which suggests that $D_{H_2O}^{peridotite/carb_melt}$ may be similar to that for CO_2-poor basalt. An experimental estimate of $D_{H_2O}^{peridotite/basalt}$ is ~0.009 (Aubaud et al., 2004). Thus, if H_2O had no influence on production of carbonated silicate partial melts, 0.3% melting would extract 25%–30% of the H_2O initially in the peridotite matrix, depending on whether melting is a batch or fractional process (Fig. 1). Thus, carbonated silicate melting likely incites significant dehydration beneath ridges at depths greater than those resulting from the influence of H_2O alone. However, this analysis does not account for enhanced melting owing to formation of hydrous carbonated silicate melt.

The combined effects of CO_2 and H_2O can be estimated by adding our function for the enhancement of melting by CO_2 (equation 1) with the parameterization of Aubaud et al. (2004) for the effect of H_2O on freezing point depression of peridotite. In this case, the onset of silicate melting (i.e., melts with <25% CO_2, corresponding to F = 0.04% for 100 ppm bulk CO_2) occurs ~185 °C below the volatile-free solidus, and 0.2 wt% melting is reached ~70 °C below (Fig. 1). Resulting dehydration of the matrix peridotite could be significant, with as much as 70% of the H_2O extracted into the melt ~20 °C below the volatile-free solidus. These estimates have considerable uncertainty and experiments are needed to quantify the combined effects of H_2O and CO_2 on small-degree melting of peridotite. Also, quantifying the influence of H_2O and CO_2 relies on their concentrations in the subridge mantle, concentrations that are not known with certainty. However, the key point is that H_2O + CO_2 together are likely to induce small degree melting and peridotite dehydration at temperatures well below those required by CO_2 or H_2O individually.

Volatile-induced melting of peridotite beneath ridges also probably depends critically on the dynamics of melt extraction. Carbonatite partial melts may be removed from their matrix beginning as deep as 300 km (Dasgupta and Hirschmann, 2006), leaving behind a residue that is virtually carbon free. In this case, carbonated silicate melting and associated dehydration may not occur by direct decompression of upwelling peridotite matrix. However, such melts can be generated by reaction between peridotite with nominally anhydrous minerals and carbonated melts ascending from their deep sources (Fig. 4). This will commence at depths similar to those where in situ carbonated silicate melting could occur. If ascending carbonatite melts percolate pervasively through overlying peridotite, such melting may occur broadly. However, if the carbonatites are segregated into channels, the melting may be spatially restricted and locally much more extensive.

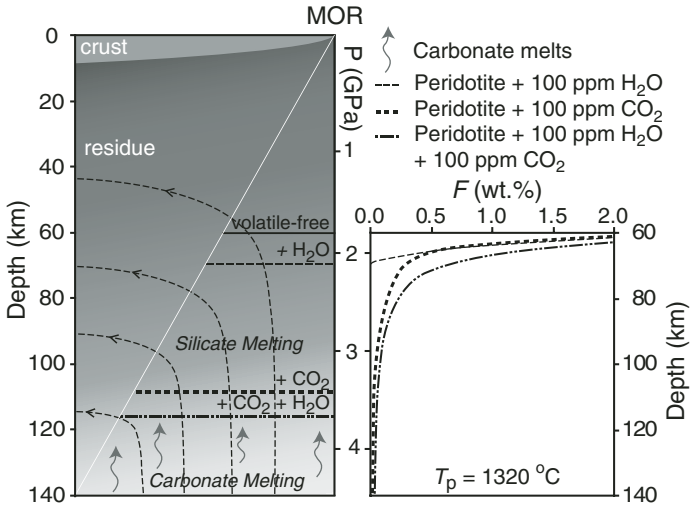


Figure 4. Schematic illustration of volatile-induced incipient silicate melting beneath mid-ocean ridges (MORs). Triangular melting regime (to left) beneath MOR showing depth of volatile-free peridotite solidus, peridotite solidus with 100 ppm H_2O (e.g., Katz et al., 2003; Aubaud et al., 2004), and estimated depths of transition from carbonatite to CO_2-rich silicate melts in peridotite owing to CO_2 alone and to CO_2 + H_2O. If carbon is completely extracted by partial melting of carbonated peridotite at great depths (Dasgupta and Hirschmann, 2006), carbonated silicate melts will be generated by reaction between peridotite and carbonated melts ascending from their deep sources. Depth vs. melt fraction curves (to right) show estimated incipient melt generation from peridotite aided by 100 ppm CO_2 (thick dashed curve), 100 ppm H_2O (thin dashed curve), and 100 ppm CO_2 + 100 ppm H_2O (dash-dot curve).

Detailed data on melt fractions from carbonated peridotite are available only at 3 GPa. If the observed temperature-melt fraction relations do not vary strongly with pressure, the depths of carbonated silicate melting beneath ridges can be estimated by comparing a mantle adiabat to isopleths of constant melt fraction assumed to be parallel to the nominally volatile-free peridotite solidus (Hirschmann, 2000). If the influence of H_2O is neglected, then for upwelling mantle that would otherwise cross the volatile-free solidus at 60 km, carbonated silicate melting would commence at 110 km and 0.2% melting will be reached at ~75 km. The combined effect of CO_2 and H_2O increases these depths to 120 km and ~82 km, respectively (Fig. 4). Thus, the combined effects of H_2O and CO_2 likely play a critical role in deep silicate melting, dehydration, and strengthening of mantle upwelling beneath ridges. Deep silicate melting initiated by CO_2 + H_2O may also be a principal source of geochemical signatures in MORB that are attributable to deep small-degree melts (Asimow and Langmuir, 2003), potentially including trace element signatures indicative of separation of melt from a garnet-bearing source (Salters and Hart, 1989).

ACKNOWLEDGMENTS

We thank Paul Asimow and Charlie Langmuir for thoughtful reviews and Tina Niemi for helpful editorial comments. This work was supported by National Science Foundation grants EAR-0310142 and OCE-0623550.

REFERENCES CITED

Asimow, P.D., and Langmuir, C.H., 2003, The importance of water to oceanic mantle melting regimes: Nature, v. 421, p. 815–820, doi: 10.1038/nature01429.

Aubaud, C., Hauri, E.H., and Hirschmann, M.M., 2004, Hydrogen partition coefficients between nominally anhydrous minerals and basaltic melts: Geophysical Research Letters, v. 31, p. L20611, doi: 10.1029/2004GL021341.

Bell, D.R., Rossman, G.R., Maldener, J., Endisch, D., and Rauch, F., 2003, Hydroxide in olivine: A quantitative determination of the absolute amount and calibration of the IR spectrum: Journal of Geophysical Research, v. 108, p. 2105, doi: 10.1029/2001JB000679.

Braun, M.G., Hirth, G., and Parmentier, E.M., 2000, The effects of deep damp melting on mantle flow and melt generation beneath mid-ocean ridges: Earth and Planetary Science Letters, v. 176, p. 339–356, doi: 10.1016/S0012–821X(00)00015–7.

Choblet, G., and Parmentier, E.M., 2001, Mantle upwelling and melting beneath slow spreading centers: Effects of variable rheology and melt productivity: Earth and Planetary Science Letters, v. 184, p. 589–604, doi: 10.1016/S0012–821X(00)00330–7.

Dasgupta, R., and Hirschmann, M.M., 2006, Melting in the Earth's deep upper mantle caused by carbon dioxide: Nature, v. 440, p. 659–662, doi: 10.1038/nature04612.

Dasgupta, R., Hirschmann, M.M., and Dellas, N., 2005, The effect of bulk composition on the solidus of carbonated eclogite from partial melting experiments at 3 GPa: Contributions to Mineralogy and Petrology, v. 149, p. 288–305, doi: 10.1007/s00410–004–0649–0.

Denbigh, K.G., 1981, The principles of chemical equilibrium: With applications in chemistry and chemical engineering: Cambridge, Cambridge University Press, 516 p.

Evans, R.L., Tarits, P., Chave, A.D., White, A., Heinson, G., Filloux, J.H., Toh, H., Seama, N., Utada, H., Booker, J.R., and Unsworth, M.J., 1999, Asymmetric electrical structure in the mantle beneath the east Pacific rise at 17 S: Science, v. 286, p. 752–756, doi: 10.1126/science.286.5440.752.

Evans, R.L., Hirth, G., Baba, K., Forsyth, D., Chave, A., and Mackie, R., 2005, Geophysical evidence from the MELT area for compositional controls on oceanic plates: Nature, v. 437, p. 249–252, doi: 10.1038/nature04014.

Forsyth, D.W., Webb, S.C., Dorman, L.M., and Shen, Y., 1998, Phase velocities of Rayleigh waves in the MELT experiment on the East Pacific Rise: Science, v. 280, p. 1235–1238, doi: 10.1126/science.280.5367.1235.

Hauri, E.H., Gaetani, G.A., and Green, T.H., 2006, Partitioning of water during melting of the Earth's upper mantle at H_2O undersaturated conditions: Earth and Planetary Science Letters, v. 248, p. 715–734, doi: 10.1016/j.epsl.2006.06.014.

Hirose, K., 1997, Partial melt compositions of carbonated peridotite at 3 GPa and role of CO_2 in alkali-basalt magma generation: Geophysical Research Letters, v. 24, p. 2837–2840, doi: 10.1029/97GL02956.

Hirschmann, M.M., 2000, The mantle solidus: Experimental constraints and the effect of peridotite composition: Geochemistry, Geophysics, Geosystems, v. 1, p. 2000GC000070.

Hirschmann, M.M., Asimow, P.D., Ghiorso, M.S., and Stolper, E.M., 1999, Calculation of peridotite partial melting from thermodynamic models of minerals and melts. III. Controls on isobaric melt productivity and the effect of water on melt production: Journal of Petrology, v. 40, p. 831–851.

Hirth, G., and Kohlstedt, D.L., 1996, Water in the oceanic upper mantle: Implications for rheology, melt extraction and the evolution of the lithosphere: Earth and Planetary Science Letters, v. 144, p. 93–108, doi: 10.1016/0012–821X(96)00154–9.

Katz, R.F., Spiegelman, M., and Langmuir, C.H., 2003, A new parameterization of hydrous mantle melting: Geochemistry, Geophysics, Geosystems, v. 4, p. 1073, doi: 10.1029/2002GC000433.

Marty, B., and Tolstikhin, I.N., 1998, CO_2 fluxes from mid-ocean ridges, arcs and plumes: Chemical Geology, v. 145, p. 233–248, doi: 10.1016/S0009–2541(97)00145–9.

Michael, P.J., 1988, The concentration, behavior and storage of H_2O in the suboceanic upper mantle: Implications for mantle metasomatism: Geochimica et Cosmochimica Acta, v. 52, p. 555–566, doi: 10.1016/0016–7037(88)90110-X.

Papale, P., 1999, Modelling of the solubility of a two-component H_2O+CO_2 fluid in silicate liquid: American Mineralogist, v. 84, p. 477–492.

Salters, V.J.M., and Hart, S.R., 1989, The hafnium paradox and the role of garnet in the source of mid ocean ridge basalts: Nature, v. 342, p. 420–422, doi: 10.1038/342420a0.

Shcheka, S.S., Wiedenbeck, M., Frost, D.J., and Keppler, H., 2006, Carbon solubility in mantle minerals: Earth and Planetary Science Letters, v. 245, p. 730–742, doi: 10.1016/j.epsl.2006.03.036.

Walter, M.J., 1998, Melting of garnet peridotite and the origin of komatiite and depleted lithosphere: Journal of Petrology, v. 39, p. 29–60, doi: 10.1093/petrology/39.1.29.

Wendlandt, R.F., and Mysen, B.O., 1980, Melting phase relations of natural peridotite+CO_2 as a function of degree of partial melting at 15 and 30 kbar: American Mineralogist, v. 65, p. 37–44.

Manuscript received 5 April 2006
Revised manuscript received 14 September 2006
Manuscript accepted 25 September 2006

Printed in USA